Defect-Mediated Phase Transitions in Active Soft Matter

Christoph A. Weber, Christopher Bock, and Erwin Frey
Arnold Sommerfeld Center for Theoretical Physics and Center for NanoScience, Department of Physics, Ludwig-Maximilians-Universität München, Theresienstraße 37, D-80333 Munich, Germany
(Received 23 October 2013; revised manuscript received 9 March 2014; published 25 April 2014)

How do topological defects affect the degree of order in active matter? To answer this question we investigate an agent-based model of self-propelled particles, which accounts for polar alignment and short-ranged repulsive interactions. For strong alignment forces we find collectively moving polycrystalline states with fluctuating networks of grain boundaries. In the regime where repulsive forces dominate, the fluctuations generated by the active system give rise to quasi-long-range transitional order, but—unlike the thermal system—without creating topological defects.

DOI: 10.1103/PhysRevLett.112.168301 PACS numbers: 82.70.Dd, 61.30.Cz, 61.50.Ah, 61.72.Lk

For a system in thermodynamic equilibrium, phases with a broken continuous symmetry in two spatial dimensions are prohibited by general theorems [1,2]. Yet, for two-dimensional solids, XY magnets, and superfluids there is a clear qualitative difference between a low-temperature phase exhibiting quasi-long-range order and a high-temperature phase where correlation functions decay exponentially [3]. Since for crystalline solids the low- and high-temperature phases are separated by two broken symmetries, namely, translational and orientational symmetry, melting can proceed by two steps [4–7]: The unbinding of dislocation pairs drives a continuous phase transition from a crystalline phase with quasi-long-range translational order into a hexatic phase [6,7] with remaining quasi-long-range bond orientational order. This is followed by another continuous transition into a disordered liquid phase mediated by the proliferation of isolated disclinations.

These statements may no longer remain valid for systems driven out of thermodynamic equilibrium. Indeed, for active systems where individual particles are self-propelled, an antagonism between dissipative processes favoring "ferromagnetic" alignment of the particles' velocities and noise can trigger a phase transition from an isotropic to a long-range ordered polar state, where particles move collectively. This was first demonstrated by Vicsek *et al.* [8] who employed a two-dimensional agent-based model where particle alignment is implemented as an update rule: Each particle aligns parallel to the average of all particles' orientations within some defined finite neighborhood. Interestingly, computer simulations of the Viscek model show that the transition is discontinuous, and the polar state exhibits propagating wavelike excitations [9,10]. The basic mechanism for the phase transition is believed to constitute a low-density phenomenon that is amenable to a kinetic description [11–15]. It assumes that the formation of order is driven by a gradual reduction in the spread of particle orientations by means of weakly aligning binary collisions. Experimental investigations supporting this picture are motility assays where cytoskeletal filaments are propelled by a lawn of molecular motors [16–19], and vibrated granular systems [20,21].

In contrast, much less is known about ordered states of active matter at high densities, where, in addition to polar order, the active system may also exhibit different degrees of liquid crystalline [22] or even crystalline order. Numerical studies of models for (self-)propelled particles discovered jammed [23], and also crystallinelike states at large packing fractions [9,24]. Recently, a mean-field theory combining elements from phase-field models of crystals [25] and hydrodynamic theories of active systems [26–28] was proposed and shown to exhibit a wealth of crystalline states of different symmetry and degrees of polar order [29]. Although all these theoretical studies suggest the interesting possibility of the emergence of translational and orientational order in active particle systems, a characterization of the nature of these ordered states and the transition between them remains elusive. In this context, one might suppose that topological defects will play an important role. Indeed, recent experimental and theoretical studies of active liquid crystals [22,30,31] show that activity leads to generation and swarming of topological defects. Active dislocations have also been shown to drive growth of bacterial cell walls through dislocation climb [32].

Here we investigate the role of topological defects for the nature of ordered states in active matter at high densities. To this end, we build on a generalized Vicsek model introduced by Grégoire and Chaté [9,33], which accounts for alignment as well as short-ranged repulsive interactions. Depending on their relative strength we find different degrees of crystalline and polar order. In the repulsion-dominated regime we find no polar order, i.e., no collective motion of the particles. Interestingly, however, fluctuations generated by the active system lead to an intriguing state of matter exhibiting quasi-long-range translational order

but—unlike systems in thermal equilibrium—devoid of any topological defects. In contrast, in the regime where dissipative alignment dominates we find collectively moving polycrystalline states with hexagonally ordered crystalline domains of characteristic size. These states exhibit pronounced defect fluctuations and sound-wave-like excitations.

To study active soft matter at high densities, we consider an off-lattice system of N particles which have a tendency to align their velocity with neighboring particles and repel each other if they come too close [9,33]. These interactions are implemented by the following parallel update rules for the velocity $\vec{v}_i(t)$ and position $\vec{x}_i(t)$ of each particle i with some discrete time interval Δt:

$$\vec{v}_i(t+\Delta t) = v_a \frac{\sum_{j\in\mathcal{A}_i} \vec{n}_j(t)}{|\sum_{j\in\mathcal{A}_i} \vec{n}_j(t)|} + v_r {\sum_{j\in\mathcal{A}_i}}' \frac{\vec{x}_{ij}(t)}{|\vec{x}_{ij}(t)|}, \quad (1)$$

$$\vec{x}_i(t+\Delta t) = \vec{x}_i(t) + \vec{v}_i(t+\Delta t)\Delta t. \quad (2)$$

Here, $\vec{n}_i := \vec{v}_i/|\vec{v}_i|$ denotes the particle director, and $\vec{x}_{ij} := \vec{x}_i - \vec{x}_j$ signifies the relative position vector between particles i and j. The first term in Eq. (1) is an alignment interaction as introduced by Vicsek *et al.* [8], where the updated velocity of particle i is given by the average velocity of all particles within a circular area $\mathcal{A}_i$ of radius $2R$ centered on particle i. The parameter v_a characterizes the strength of alignment as well as the particles' propulsion speed. The second term in Eq. (1) describes a soft, pairwise additive repulsive interaction between a given particle i and all its neighbors within the same area $\mathcal{A}_i$. It displaces a particle pair, whose separation $|\vec{x}_{ij}(t)| \leq 2R$ [$i \neq j$, indicated by the primed sum], radially outward by a constant amount $v_r\Delta t$. In the following, we will refer to R as the particle radius. Length and time are measured in units of the particle diameter, $2R$, and the corresponding time to traverse this distance, $\tau = 2R/v_a$, respectively. The model can easily be generalized to account for different radii for alignment and repulsion, R_a and R_r, respectively. Here, we focus on the competition between alignment and repulsion, and therefore have chosen the two radii as $2R_r = R_a$; previous studies of the Vicsek model with repulsion were restricted to the limit $R_r \ll R_a$ [34,35]. We are mainly interested in the collective dynamics as a function of the packing fraction $\rho = N\pi R^2/L^2$, and the relative strength of the repulsive and alignment interaction $\nu := v_r/v_a$.

First, we analyze the degree of polar and bond-orientational order. The global polarization is defined as a system average $\langle\ldots\rangle_i$ over all particle orientations $\vec{n}_i(t)$: $\mathcal{P}(t) = |\langle\vec{n}_i(t)\rangle_i|$. Local bond-orientational order is characterized by the hexatic order parameter $\Psi_{6,i} = |\mathcal{N}_i|^{-1}\sum_{j\in\mathcal{N}_i} e^{\imath 6\theta_{ij}}$, where summation extends over all $\mathcal{N}_i$ topological (Voronoi) nearest neighbors of particle i, and θ_{ij} is the "bond" angle between particles i and j relative to an arbitrarily chosen reference axis.

Figures 1(a) and 1(b) illustrate the degree of polar and hexatic order as a function of the packing fraction ρ, and the relative strength of repulsive and alignment interactions ν. We observe that global polar order, characterized by the time-averaged polarization $P = \langle\mathcal{P}(t)\rangle_t$ [$\langle\ldots\rangle_t$: time average], is well established for weak repulsion $\nu \lesssim 1$, but at $\nu \approx 1$ sharply drops to very small values [Fig. 1(a)]. The respective phase boundary between polar and unpolarized states is tentatively defined by $P = 0.2$. Note that it is nearly independent of the packing fraction ρ, indicating that the transition from a polar collectively moving state to an unpolarized state is mainly driven by an antagonism between repulsive and alignment forces but not the particle density. To discern the different degrees of bond-orientational or translational order is more difficult. As can be inferred from Fig. 1(b), there are different degrees of global hexatic order, $\Psi_6 = \langle|\langle\Psi_{6,i}\rangle_i|\rangle_t$, with a maximum for large packing fraction ρ and strong repulsive interaction (large ν); the dashed white line in Fig. 1(b) corresponds to a value of $\Psi_6 = 0.2$. Strikingly, the loss of polar order is concomitant with the emergence of a high degree of crystalline order, and vice versa.

While the global polar and hexatic order parameters provide a first rough estimate of the degree and nature of the ordered states, a full characterization thereof requires an in-depth analysis of the spatiotemporal dynamics. In particular, as for thermodynamic equilibrium systems, the dynamics and the spatial organization of topological defects are especially important indicators of crystalline order. Figures 1(c)–1(e) depict snapshots of the local

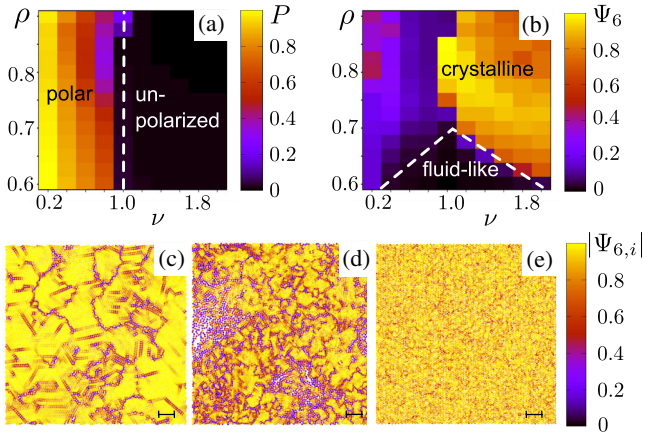

FIG. 1 (color online). Global polar order parameter P (a) and hexatic order parameter Ψ_6 (b) as a function of the control parameters ρ and ν. The dashed white lines indicate tentative boundaries between polar and unpolarized states, and crystalline states exhibiting crystalline order from fluidlike states. Snapshots of local hexatic order $|\Psi_{6,i}|$ for a relative interaction value $\nu = 0.25$ (c), $\nu = 0.75$ (d), and $\nu = 1.5$ (e); all three snapshots correspond to a high packing fraction of $\rho = 0.85$. See also videos in the Supplemental Material [36]. Scale bars indicate a distance of $20R$.

hexatic order $|\Psi_{6,i}|$ at a large packing fraction of $\rho = 0.85$ for a set of values for ν. Depending on the relative strength of repulsive and alignment interaction marked differences in the spatial organization of defects are clearly visible. While for $\nu \lesssim 0.25$ dislocations align to form a network of rather well-defined grain boundaries, they tend to cluster in the intermediate regime $0.375 \lesssim \nu \lesssim 1.0$ [Figs. 1(c), 1(d)]. For $\nu \gtrsim 1.0$, concomitant with the loss of polar order, the defects become more evenly spread and slowly disappear from the system; see Fig. 1(e) for a snapshot, and Fig. 2(a) for the dynamics of the defect density. This reassures the observation made on the basis of the order parameters, namely, that polar and crystalline order are mutually exclusive.

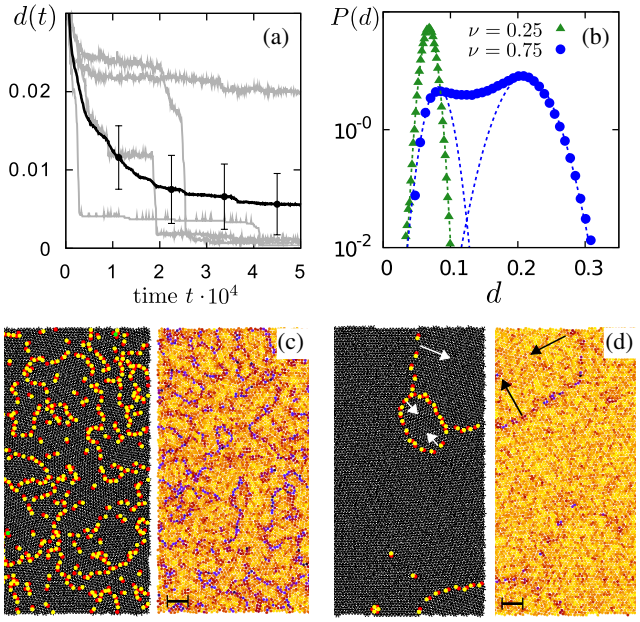

FIG. 2 (color online). (a) Defect ratio $d(t)$ as a function of time t for $(\rho, \nu) = (0.85, 1.5)$. The black curve is an average over 50 realizations (gray lines) with error bars indicating the standard deviation. The steep decline in the time traces corresponds to the fast annihilation processes of grain boundaries [see (d), white errors]. (b) Probability distribution $P(d)$ [lin(d)-log] of the defect ratio for two stationary (flowing) polycrystalline states, i.e., $(\rho, \nu) = (0.85, 0.25)$ (green, triangles) and $(\rho, \nu) = (0.85, 0.75)$ (blue, circles). (c),(d) Snapshots illustrating the defect dynamics for an active crystal $[(\rho, \nu) = (0.85, 1.5)]$, where the system shows a high degree of crystalline order. (c) Early phase with roughly homogeneous distributed defects and small hexagonal patches. (d) Formation of ringlike grain boundaries at larger times that contract (indicated by black arrows), leading to a sudden decrease of $d(t)$ [see (a)]. The left and right half of each figure depict the *Voronoi* triangulation and the local hexatic order parameter $|\Psi_{6,i}|$, respectively. Disclinations are indicated by red and yellow dots, and green dots corresponds to particles with more than sevenfold or less than fivefold coordination. Scale bars: $20R$.

The intricate interplay between crystalline and polar order is elucidated by the spatiotemporal dynamics of the defects; see the videos in the Supplemental Material [36]. For $\nu \lesssim 0.375$, we observe a flowing polycrystalline state where changes in the flow direction strongly affect the network of grain boundaries. In the stationary regime, the defect fraction $d = D/N$ is Gaussian distributed around a mean of about 7% [Fig. 2(b)]; here D is the number of all particles with a coordination different from sixfold. In the intermediate regime, we find intermittent dynamics where episodes of polycrystalline and polar order alternate with episodes of disorder which are accompanied by sound waves (see Supplemental Material [36], S1, S4). These compression waves, caused by collisions of polar crystalline domains, impede their growth into larger domains and thereby rule out the coexistence of polar and crystalline order. Moreover, the intermittent dynamics is also reflected in a bimodal shape of the defect probability density $P(d)$ [Fig. 2(b)]: While the peak at low values of d corresponds to particle configurations with a high degree of polar order, the peak at higher values originates from time intervals, where collective motion breaks down and strong density inhomogeneities arise.

Dynamics and spatial organization of topological defects change qualitatively for strong repulsive interaction, $\nu \gtrsim 1$, where polar order is also absent. Starting from an initial disordered state [Fig. 2(c)], we observe that first the spatial distribution of defects coarsens quickly and then organizes into grain boundaries [Fig. 2(d)]. Subsequently, these grain boundaries contract and self-annihilate, leaving the system in a state with evenly spread disclinations and dislocations; see also videos in the Supplemental Material [36]. The ringlike annihilation processes of these grain boundaries are seen as periods of steep decline in the time traces for the defect fraction [Fig. 2(a), gray curves]. After each steep decline, the decrease in defect number slows down significantly due to an enlarged interdefect distance. We observe that the number of isolated defects decreases extremely slowly; see the asymptotic decline in the average defect fraction in Fig. 2(a). Moreover, we find evidence that the topological defects even move subdiffusively (see Supplemental Material [36], S3). Taken together, it is numerically not feasible to study the asymptotic dynamics significantly beyond what is shown in Fig. 2(a). To check whether a defect-free crystal is stable we initialized the system in an unpolarized and perfectly hexagonal ordered state, and waited until the global hexatic order parameter $\Psi_6(t)$ converged to a stationary value. Even though the active dynamics leads to a reduction of the hexatic order parameter to a stationary value of $\Psi_6 \approx 0.9$, it is not strong enough to create any defects for densities larger than $\rho \approx 0.8$. Hence, we conclude that the stationary states for $\nu \gtrsim 1$ and large density ($\rho \gtrsim 0.8$) are indeed free of topological defects. When decreasing the packing fraction below 0.8, there is a small range of packing fractions where

fluctuations trigger the creation of defects (see Supplemental Material [36], S2). However, in the ensuing nonequilibrium steady states corresponding to this smallish transitional region, dislocations are always found in pairs. As in the case of thermal systems this would indicate that the corresponding states also exhibit quasi-long-range order. Exploring parameter space we could not identify hexatic phases with isolated dislocations. Further decreasing the packing fraction, the defect ratio $d(\rho)$ increases to a rather high value $d \sim 0.4$, signaling a transition to a fluidlike phase.

In order to further scrutinize the nature of order within the crystalline regime we computed the pair correlation function $g(\vec{r})$, the corresponding static structure factor $S(\vec{q})$, and the correlation functions [3,36]

$$C_\alpha(r) = \frac{1}{\sum_i |\Psi_{\alpha,i}|^2} \sum_{|\vec{x}_i - \vec{x}_j| = r} \Psi_{\alpha,i} \Psi^*_{\alpha,j} \tag{3}$$

for the hexatic $\Psi_{6,i}$, and the translational $\Psi_{\vec{G},i} = e^{-\imath \vec{G} \vec{r}_i}$ order parameter with $\vec{G}$ denoting a reciprocal lattice vector. As discussed above, for $\nu > 1$, dislocations vanish extremely slowly and, as a consequence, the asymptotic nonequilibrium steady state cannot be reached within a computationally accessible time. Therefore, to obtain steady state results for the correlation functions, we initialized the system in a hexagonal and isotropic configuration ($\Psi_6 = 1$, $P \approx 0$); the corresponding results for simulations starting from a disordered initial state are discussed in the Supplemental Material [36]. We find that both $S(\vec{q})$ [Figs. 3(a) and 3(b)] and $g(\vec{r})$ (see Supplemental Material [36], S5) exhibit a sharp and discrete pattern of hexagonal symmetry, clearly indicating a high degree of translational order. This is confirmed by $C_6(r)$ being constant over the whole system size [Fig. 3(c)], and the slow decay of the translational correlation function $C_{\vec{G}}(r)$. The decay follows a power law with a very small exponent of about 0.04 [see Fig. 3(d), dashed gray line], which is difficult to discern from a logarithmic decay. Taken together, these results lead us to conclude that this state of active matter is an active crystal, free of topological defects with long-range bond-orientational order and quasi-long-range translational order. In contrast, in the parameter regime of polycrystalline order, the static structure factor shows the ringlike features of a liquid [Fig. 3(b)]; see also Supplemental Material [36], S5. These features are due to the different orientations of the hexagonally ordered patches, as also evident from the exponential decay in C_6 [Fig. 3(c)] and the fast decay of $C_{\vec{G}}(r)$ [Fig. 3(e)].

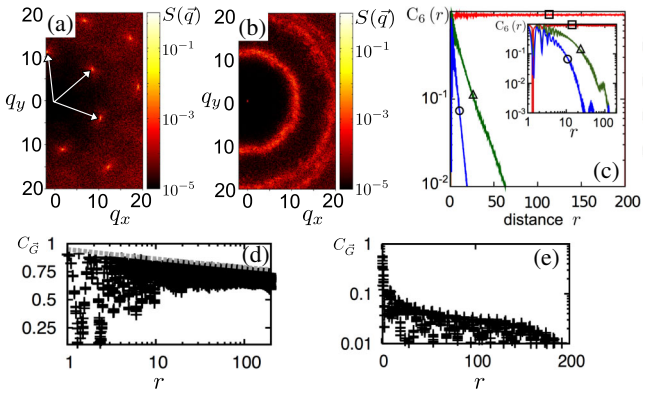

FIG. 3 (color online). Static structure factor $S(\vec{q})$ for (a) the active crystal $[(\rho, \nu) = (0.85, 1.5)]$ and (b) a polycrystal $[(\rho, \nu) = (0.85, 0.25)]$, respectively, both in the stationary regime. Reciprocal lattice vectors $\vec{G}$ are indicated by white arrows. (c) Correlation function $C_6(r)$ in lin(r)-log (inset: log-log) for the same parameters as in Figs. 1(c)–(d): $\rho = 0.85$, and $\nu = 1.5$ (red, square), $\nu = 0.75$ (blue, circle), and $\nu = 0.25$ (green, triangle). Correlation function $C_{\vec{G}}(r)$ for $(\rho, \nu) = (0.85, 1.5)$ (d) [log(r)-lin, dashed line is a power law with exponent 0.04] and $(\rho, \nu) = (0.85, 0.25)$ (e). All results correspond to a simulation box of size $L = 400$ containing $N = 172\,156$ particles; see Supplemental Material [36] for the data evaluation.

Topological defects are the hallmark of phase transitions in two-dimensional crystalline systems. For systems in thermodynamic equilibrium they drive the successive breaking of translational and bond-orientational order. Our investigations of active crystalline matter at high density have revealed that while defects still play a decisive role, the emerging defect dynamics and phase behavior differ qualitatively from their equilibrium analogues. In active systems, the nonequilibrium steady states include different types of polycrystalline phases, and a crystalline phase with quasi-long-range translational order but completely devoid of any topological defects. How the genuine differences of the fluctuations generated by the active particle motion compared to thermal fluctuations permit a defect-free state remains presently unclear and constitutes an interesting future challenge for a continuous theory describing the defect dynamics in polar active matter. One possibility is to develop a Langevin description for the defect dynamics including interaction potentials that can be directly measured in the simulations. In regimes where defects are sparse, an alternative promising route might be to employ kinetic approaches [11,12,14,15].

Our predictions can readily be tested by experimental model systems which may, for instance, be realized using emulsion droplets containing extensile microtubule bundles [22]. They exhibit spontaneous motility when in frictional contact with a hard surface; depending on the availability of adenosine triphosphate their motion can be tuned from passive Brownian motion to active persistent random walks. We envisage that large assemblies of such active soft droplets are ideal model systems to test our theoretical predictions. Though the detailed mechanisms of the interaction between the droplets is different from the interaction rules of the agent-based model, we expect the main features of the dynamics and phase behavior to be generic for active matter at high densities. Another promising experimental system is active colloidal particles. Recent studies of

photoactivated colloidal particles [37] and carbon-coated Janus particles [38] show various types of pattern and cluster formation. The versatility of colloidal systems should also allow the design of experiments to explore the dynamics of active matter at high density.

We would like to thank David Nelson for fruitful and stimulating discussions. This project was supported by the Deutsche Forschungsgemeinschaft in the framework of the SFB 863, and the German Excellence Initiative via the program "NanoSystems Initiative Munich" (NIM).

[1] N. D. Mermin and H. Wagner, Phys. Rev. Lett. **17**, 1133 (1966).
[2] P. Hohenberg, Phys. Rev. **158**, 383 (1967).
[3] D. R. Nelson, *Defects and Geometry in Condensed Matter Physics* (Cambridge University Press, Cambridge, England, 2002), p. 392.
[4] J. M. Kosterlitz and D. J. Thouless, J. Phys. C **6**, 1181 (1973).
[5] A. P. Young, Phys. Rev. B **19**, 1855 (1979).
[6] B. I. Halperin and D. R. Nelson, Phys. Rev. Lett. **41**, 121 (1978).
[7] D. R. Nelson and B. I. Halperin, Phys. Rev. B **19**, 2457 (1979).
[8] T. Vicsek, A. Czirok, E. Ben-Jacob, I. Cohen, and O. Shochet, Phys. Rev. Lett. **75**, 1226 (1995).
[9] G. Grégoire and H. Chaté, Phys. Rev. Lett. **92**, 025702 (2004).
[10] H. Chaté, F. Ginelli, G. Grégoire, and F. Raynaud, Phys. Rev. E **77**, 046113 (2008).
[11] E. Bertin, M. Droz, and G. Grégoire, Phys. Rev. E **74**, 022101 (2006).
[12] E. Bertin, M. Droz, and G. Grégoire, J. Phys. A **42**, 445001 (2009).
[13] C. A. Weber, F. Thüroff, and E. Frey, New J. Phys. **15**, 045014 (2013).
[14] F. Thüroff, C. A. Weber, and E. Frey, Phys. Rev. Lett. **111**, 190601 (2013).
[15] T. Hanke, C. A. Weber, and E. Frey, Phys. Rev. E **88**, 052309 (2013).
[16] T. Butt, T. Mufti, A. Humayun, P. B. Rosenthal, S. Khan, S. Khan, and J. E. Molloy, J. Biol. Chem. **285**, 4964 (2010).
[17] V. Schaller, C. Weber, C. Semmrich, E. Frey, and A. R. Bausch, Nature (London) **467**, 73 (2010).
[18] V. Schaller, C. Weber, E. Frey, and A. R. Bausch, Soft Matter **7**, 3213 (2011).
[19] Y. Sumino, K. H. Nagai, Y. Shitaka, D. Tanaka, K. Yoshikawa, H. Chaté, and K. Oiwa, Nature (London) **483**, 448 (2012).
[20] J. Deseigne, O. Dauchot, and H. Chaté, Phys. Rev. Lett. **105**, 098001 (2010).
[21] C. A. Weber, T. Hanke, J. Deseigne, S. Léonard, O. Dauchot, E. Frey, and H. Chaté, Phys. Rev. Lett. **110**, 208001 (2013).
[22] T. Sanchez, D. T. N. Chen, S. J. DeCamp, M. Heymann, and Z. Dogic, Nature (London) **491**, 431 (2012).
[23] S. Henkes, Y. Fily, and M. C. Marchetti, Phys. Rev. E **84**, 040301 (2011).
[24] J. Bialké, T. Speck, and H. Löwen, Phys. Rev. Lett. **108**, 168301 (2012).
[25] K. R. Elder, M. Katakowski, M. Haataja, and M. Grant, Phys. Rev. Lett. **88**, 245701 (2002).
[26] J. Toner and Y. Tu, Phys. Rev. Lett. **75**, 4326 (1995).
[27] J. Toner and Y. Tu, Phys. Rev. E **58**, 4828 (1998).
[28] J. Toner, Phys. Rev. E **86**, 031918 (2012).
[29] A. M. Menzel and H. Löwen, Phys. Rev. Lett. **110**, 055702 (2013).
[30] L. Giomi, M. J. Bowick, X. Ma, and M. C. Marchetti, Phys. Rev. Lett. **110**, 228101 (2013).
[31] L. M. Pismen, Phys. Rev. E **88**, 050502 (2013).
[32] A. Amir and D. R. Nelson, Proc. Natl. Acad. Sci. U.S.A. **109**, 9833 (2012).
[33] G. Grégoire, H. Chaté, and Y. Tu, Physica (Amsterdam) **181D**, 157 (2003).
[34] H. Chaté, F. Ginelli, G. Grégoire, F. Peruani, and F. Raynaud, Eur. Phys. J. B **64**, 451 (2008).
[35] L. Peng, Y. Zhao, B. Tian, J. Zhang, B.-H. Wang, H.-T. Zhang, and T. Zhou, Phys. Rev. E **79**, 026113 (2009).
[36] See Supplemental Material at http://link.aps.org/supplemental/10.1103/PhysRevLett.112.168301 for videos and more information, which includes Refs. [10, 39, 40].
[37] J. Palacci, S. Sacanna, A. P. Steinberg, D. J. Pine, and P. M. Chaikin, Science **339**, 936 (2013).
[38] I. Buttinoni, J. Bialké, F. Kümmel, H. Löwen, C. Bechinger, and T. Speck, Phys. Rev. Lett. **110**, 238301 (2013).
[39] C.-C. Liu, G. S. W. Craig, H. Kang, R. Ruiz, P. F. Nealey, and N. J. Ferrier, J. Polym. Sci., Part B: Polym. Phys. **48**, 2589 (2010).
[40] E. R. Weeks and D. A. Weitz, Phys. Rev. Lett. **89**, 095704 (2002).